Deformation, stirring and material transport in thermochemical plumes

Shu-Chuan Lin[1,2] and Peter E. van Keken[1]

Received 28 May 2006; revised 2 August 2006; accepted 18 September 2006; published 19 October 2006.

[1] The deformation, stirring processes and transport structures for a series of numerical models of plume formation in axisymmetric spherical shell are examined to better understand the development of lateral heterogeneity in mantle plumes. In our models we find that under a wide range of conditions the surrounding material is heated and entrained. This indicates that plume sampling the ambient mantle material on its way to the base of the lithosphere cannot be ruled out. The deformation and convective stirring can be significantly enhanced in the thermochemical plumes and the dispersion of compositional heterogeneity can be much more effective than that in the purely thermal plumes. For models with episodic pulsations or with small-scale convection due to the interplay between the thermal and compositional buoyancy forces, material in the plume and the source region can undergo strong stretching and folding resulting in structures such as filaments, streaks, tendrils and well-mixed regions. Islands can be surrounded by highly deformed regions which may contribute to structures such as the coexistence of the compositional heterogeneity and relatively homogeneous matrix in Ocean Island Basalts (OIBs). These results may have implications for the interpretation of the lateral heterogeneities of the OIBs. **Citation:** Lin, S.-C., and P. E. van Keken (2006), Deformation, stirring and material transport in thermochemical plumes, *Geophys. Res. Lett.*, *33*, L20306, doi:10.1029/2006GL027037.

1. Introduction

[2] Recent studies show that the compositionally dense layer may be present in the lowermost mantle and significantly influence the formation of the mantle plumes, resulting in diverse and complicated plume structures [e.g., *van der Hilst and Kárason*, 1999; *Davaille*, 1999; *Farnetani and Samuel*, 2005; *McNamara and Zhong*, 2005; *Lin and van Keken*, 2006a, 2006b]. The results of the numerical experiments for plume originating from a thermochemical boundary layer frequently deviate from the classical plume head-plume tail structure. As a consequence, the deformation, transport structure, stirring processes and dynamic features might be significantly different than those in plumes with purely thermal origin. This could complicate and modify the interpretation of the chemical variations of Ocean Island Basalts (OIBs). In this study we address these problems from dynamical considerations and particularly focus on two long-lived problems. One controversial issue is whether the chemical heterogeneity is mainly inherited from the source region or the overlying mantle could also have significant contribution [e.g., *Hart et al.*, 1992; *White et al.*, 1993; *Hauri et al.*, 1994; *van Keken*, 1997; *Farnetani and Samuel*, 2005]. Another fundamental question concerns the development and destruction of the lateral heterogeneities during the process of plume formation, which relies on a better understanding of the deformation and stirring in the mantle [e.g., *Kellogg and Turcotte*, 1990; *Christensen and Hofmann*, 1994; *Schmalzl et al.*, 1996; *Ten et al.*, 1997; *Davies*, 2002; *van Keken et al.*, 2002; *Farnetani and Samuel*, 2003]. Here we use classical techniques to study deformation and stirring in mantle plumes. We examine the probability of the entrainment of overlying mantle during the plume formation by scrutinizing the deformation, temperature and advection of particles for material originally located above the thermal boundary layer at various depths. We present the deformation and stirring processes for a purely thermal plume as a reference and results for thermochemical plumes with the development of the secondary instabilities and the small-scale convection.

2. Models and Computations

[3] The plume models are a series of numerical experiments in axisymmetric, spherical geometry obtained by convection models of incompressible, Newtonian fluid at infinite Prandtl number in previous studies [*Lin and van Keken*, 2006a, 2006b]. A high resolution, finite-element mesh with resolution of $\sim$2–5 km in the thermal boundary layer and the region near model axis is used in the calculations [*Lin and van Keken*, 2006a]. In this previous work, we systematically explored the effects of the temperature-dependent viscosity (maximum viscosity contrast $\Delta\eta = 100$ and 1000), the density contrast $\Delta\rho$(0–400 kg/m^3) and the thickness d (10–200 km) of the compositionally dense layer on the formation of plumes. The buoyancy number is given by $B = \Delta\rho/\rho\alpha\Delta T$, where $\Delta\rho$ is the intrinsic density difference between the compositionally distinct material in the lowermost mantle and the overlying mantle [*Lin and van Keken*, 2006b]. The thermochemical plumes models were categorized into three representative regimes including: (i) low temperature plume with little entrainment of dense material, (ii) high temperature plume with significant entrainment of dense material, and (iii) plumes in the intermediate regime in which secondary instabilities or small-scale convection develops. Processes in plumes of regime-(i) have been studied in *Farnetani et al.* [2002] and we find that processes in regime-(ii) are basically similar to those in purely thermal plumes. Therefore, we will mainly

[1]Department of Geological Sciences, University of Michigan, Ann Arbor, Michigan, USA.
[2]Now at Department of Geosciences, National Taiwan University, Taipei, Taiwan.

0094-8276/06/2006GL027037

discuss the results of purely thermal plumes and thermochemical plumes in regime-(iii) in the following section.

[4] The mixing of heterogeneities for convective flow involves stretching, folding, breakup and diffusion [e.g., *Ottino*, 1989]. For mantle it is often noted that stirring is a more appropriate description [e.g., *Davies*, 1999] because the breakup and diffusion are negligible. Stretching and folding of material elements can be quantified by Finite-time Luyaponov exponent (FTLE) [e.g., *Ottino*, 1989; *Ferrachat and Ricard*, 1998; *van Keken et al.*, 2003], which measures the growth rate of the distance between two close Lagrangian particle trajectories by exponents. The FTLE (λ) can be expressed as

$$\lambda(x(\tau),\tau) = \frac{1}{\tau}\log\left(\frac{|\delta x(\tau)|}{|\delta x(0)|}\right) \quad (1)$$

where $\delta(\tau)$ is the distance between two points after time τ, the δx(0) is the initially separation of two points that are initially close, and the orientation of δx(0) is chosen so that one obtains the maximum value for λ.

[5] Distances between passive tracers are used as a proxy for calculation of the FTLE. We keep track of tracer pairs, which are initially distributed uniformly with a small random perturbation over the entire model domain. The imposed random perturbation is to avoid the effect of tracer aggregation [*Tackley and King*, 2003]. More than 3×10^6 pairs are used. Each tracer pair is composed of one reference particle (r_0, θ_0) and two particles (r_1, θ_1; r_2, θ_2) that have initial non-dimensional distance from the reference particle of 10^{-6} in r- and θ-direction, respectively. The distance between the particle tracers are renormalized constantly. The lengths of the line segments are calculated accordingly and the larger length of these two segments is chosen to calculate the FTLE. Advection of particles and markers is calculated using fourth-order Runge-Kutta integration with time steps determined by half of the Courant-Friedrichs-Levy criterion. We have demonstrated that error of individual trajectory is less than 0.1% for a testing model with a relatively coarse grid [*Lin and van Keken*, 2006a]. The errors of particle advections in the plume models should be significantly less than 0.1% because a high-resolution mesh is used and only relatively short time periods are considered. Even if the individual trajectories may suffer from computational errors, the behaviors of the trajectory ensembles are likely reliable [*Metcalfe et al.*, 1995]. For the details of the plume models and the techniques to calculate particle advections and to solve the equations governing the flow, we refer to previous studies [*Lin and van Keken*, 2006a, 2006b].

3. Results

[6] The distribution of FTLE of a purely thermal plume has similar characteristics with those in previous study using numerical models with $\Delta\eta = 100$ in three-dimensional Cartesian geometry [*Farnetani et al.*, 2002]. The deformation is localized (Figures 1a and 1b). The top of the plume head has large values of FTLE and large amount of stretching. The core of the plume head has the lowest values of FTLE and insignificant deformation. The plume axis also has high values of FTLE and material is stretched into thin, continuous filaments. The material of the main portion of the plume head is stretched and mildly folded. The relative values of the FTLE for material originally in the region near the plume axis in the lower mantle is larger in this study (Figure 1a). This region corresponds to the rim of the plume head (Figure 1b). This may be caused by the combined effects due to the differences of the model geometries and the viscosity contrast and the much higher resolution used in our models. The overlying mantle material in the periphery of the plume head is deformed and elongated along the stretching directions that parallel to the region with maximum FTLE in response to the compression from the ascending plume head (Figures 1c and 1e). Material keeps thinning when plume head further approaches the surface. Material at various depths in the region near the model axis is therefore closely compacted and the heating of the material at shallower depths becomes easier (Figures 1d and 1f). Most of the heated material originally in the deeper depths travels away the axis and eventually is entrained into the plume head. When the plume head approaches the upper

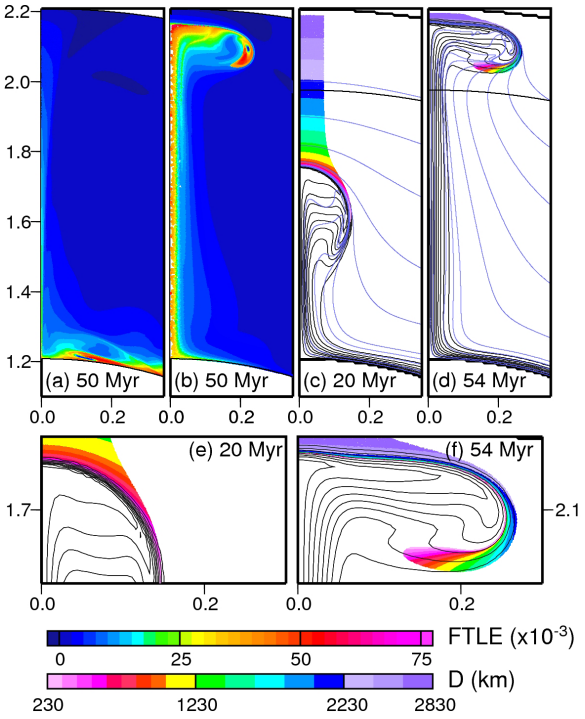

Figure 1. Results for purely thermal plume model with $\Delta\eta$ = 1000 at selected snapshots. (a, b) FTLE (λ) with non-dimensional values plotted at the initial positions and final positions, respectively. (c, d) Advection of passive tracers and the distributions of the markers chains. The distance (D) between the tracers and core-mantle boundary (CMB) is marked in the color palette. The thin blue lines are marker chains originally located at selected depths (40, 80, 150, 200, 250, 500, 885, 1385, 1815, 2215 km above CMB). Plume is depicted by the excess temperature by contours with non-dimensional interval 0.1 (0.1–0.9). (e, f) Snapshots showing that evolution of overlying mantle. The length scale in these models is rescaled by the depth of the mantle in the models (2885 km). Similar notations are used throughout the manuscript. The evolution of thermal field is referred to Figure 2b of *Lin and van Keken* [2006a].

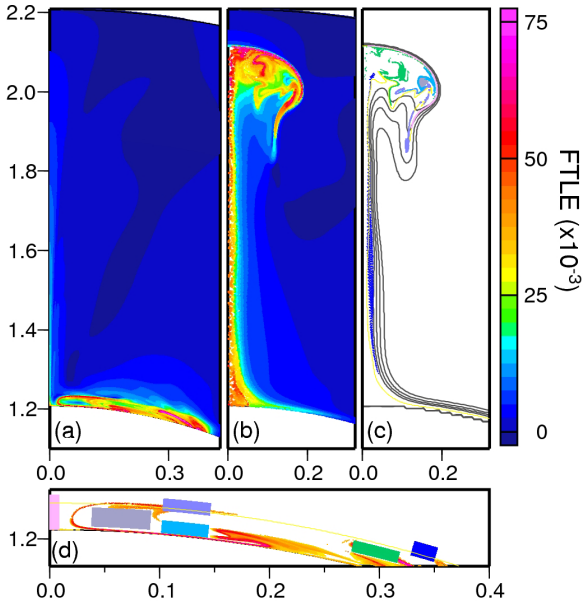

Figure 2. Results for a representative model with secondary instabilities at snapshot of 57 Myr. (a, b) FTLE with non-dimensional values plotted at the initial positions and final positions, respectively. (c) Advection of passive tracers from six regions with highest or lowest FTLE. (d) The original locations of the tracers. Regions of high value of FTLE are plotted at the background for reference. Plume is depicted by the excess temperature by contours with non-dimensional interval 0.1 (0.1–0.4). The thin yellow lines in Figures 2c and 2d mark the boundary between the ambient mantle and the regions with dense material at 57 Myr and 0 Myr, respectively. Model parameters: $\Delta\eta = 1000$, $\Delta\rho = 50$ kg/m^3, $B = 0.56$, $d = 70$ km. The evolution of thermal field is referred to Figure 3a of *Lin and van Keken* [2006b].

mantle, the upper mantle material is deformed, heated and attached to the top of plume head (Figure 1f). The upper mantle material is screened from the plume head by a thin layer with a few to a few tens kilometers of material originally in the deeper mantle (Figures 1e and 1f). The temperature is elevated for about 10–40% of the maximum thermal perturbation of thermal boundary layer. Similar behavior for entrainment of ambient mantle can be observed in models of thermochemical plumes.

[7] Figure 2 shows that the injection of secondary instabilities from the boundary layer into the existing plumes causes significant deformation (Figures 2a and 2b). The episodic pulsations have high values of FTLE and act as dynamical barriers for material transport which resembles the barrier provided by the primary plume head. In these regions stretching is the dominant process. Material undergoes significant folding when instabilities reach the plume head or subsequent one approaches. This leads to a much more efficient stirring and effective dispersion of heterogeneity. Figures 2c and 2d show the advection of passive particles in selected regions. For particles in the regions with large FTLE, the particles are stretched out to thin filaments. In some regions the filaments are distorted and folded and the filaments become tendrils or streaks. The material in the secondary instability does not interact with the surrounding mantle. The original structure can persist in the unmixed regions (Figures 2c and 2d). The dimensions of these unmixed islands range from about a few hundred of kilometers to a few kilometers. Figure 3 shows that significant deformation and stirring can be present in both the plume and thermal boundary layer when small-scale convection develops. Passive tracers originally located in distant regions are mixed together or closely compacted in the high strain regions. In the low strain region particles are rotated and deformed but remain keep their identities. The main difference in respect to stirring process is that the secondary instabilities can introduce significant deformation mainly in an episodic fashion, whereas the small-scale convection can more effectively generate folding in some cases in both the plume and the boundary layer.

[8] Figure 4 shows the lengths of marker chains at selected depths as a function of time for four representative models. The increase of length is limited to a few times of the original length of marker chains at any depths when it reaches the top boundary for purely thermal models. It can be significantly increased for the marker chains originally located in the thermochemical boundary layer when small-scale convection or secondary instabilities develop in the plumes. This is caused by the enhanced, strong stretching and folding of material leading to the drastic increase of the length between two material interfaces. Note that various maximum values of the model elapsed time are chosen in Figure 4. The time period is determined roughly by the time interval between the plume initiation and the approach of the plume head to the upper boundary.

4. Discussion

[9] We found that a substantial fraction of the surrounding mantle material at various depths can be heated and

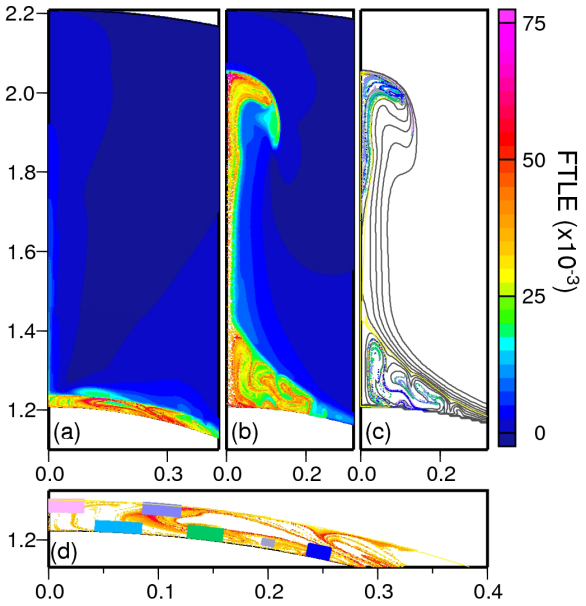

Figure 3. Similar results as in Figure 2, except for a model with small-scale convection at snapshot of 75 Myr. The thin yellow lines in Figure s 3c and 3d are marker chains initially located in 80-km depth. Model parameters: $\Delta\eta = 1000$, $\Delta\rho = 75$ kg/m^3, $B = 0.83$, $d = 80$ km. The evolution of thermal field is referred to Figure 9 of *Lin and van Keken* [2006b].

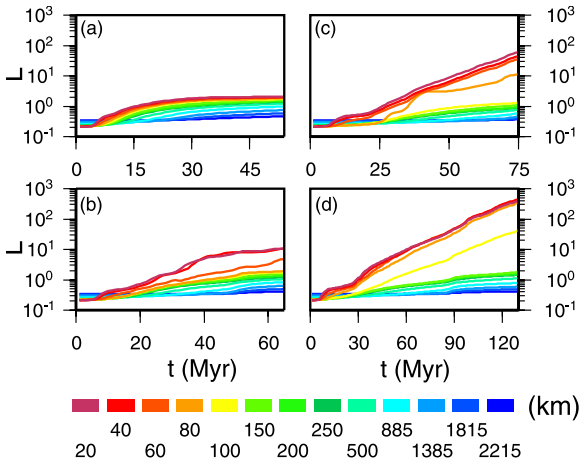

Figure 4. Temporal evolution of lengths of marker chains for regions within 10 degrees from the axis for four representative models. Shown here are nondimensional lengths (L) normalized by 2885 km. The distance from the CMB to the marker chain is marked in the color palette. (a) Purely thermal model with $\Delta\eta = 1000$. The increase in length against time for marker chains originally located in the thermal boundary layer appears to be a superlinear function during the plume initiation. It then roughly becomes a sublinear function when the plume head is established and gradually approaches to the top boundary. (b) The length-increase of marker chains has multiple phases with exponential growth rates for plume with secondary instabilities. Model parameters: $\Delta\eta = 1000$, $\Delta\rho = 50$ kg/m^3, $B = 0.56$, $d = 70$ km. (c) The lengths of the marker chains increase exponentially for plume with small-scale convection. Model parameters: $\Delta\eta = 1000$, $\Delta\rho = 75$ kg/m^3, $B = 0.83$, $d = 80$ km. (d) The lengths of the marker chains for plume with combined effects. Model parameters: $\Delta\eta = 1000$, $\Delta\rho = 65$ kg/m^3, $B = 0.72$, $d = 100$ km. The evolution of thermal field is referred to Figure 6 of *Lin and van Keken* [2006b].

attached into the plume. The entrained material can contain material at any depths with various proportions. While the core of the plume provides the largest temperature contrast with the average mantle, the entrained material is significantly heated and may contribute to melting in plumes that erupt at shallow depths near mid-ocean ridges such as cases of the Galapagos and the Iceland plume and the Kerguelen plume in its history. This suggests that the depleted MORB mantle source (DMM) and lower mantle material may contribute to the generation of OIBs under certain conditions.

[10] Although the starting model in our calculations is a two component system in terms of physical property (compositional density), lateral heterogeneities in geochemistry or composition may still be present within each component. These lateral heterogeneities may be affected by the deformation and stirring processes observed in our models, eventually resulting in the geochemical variations in the OIBs. Our models show that effective convective stirring can occur in the thermochemical plumes through strong stretching and folding. Various types of dispersal of compositional heterogeneities can occur in a single system. Structures such as streaks, filaments, tendrils and well-mixed region can be found in plumes and may contribute to the lateral heterogeneities of OIB. Islands can coincide with well-mixed regions, which may help to explain structures such as compositional heterogeneity that may be present in the relatively homogeneous matrix of OIB as proposed for Hawaiian magma [e.g., *Ren et al.*, 2005].

[11] The frontier of the plume head is a region with high stress conditions. Non-Newtonian behavior could be important [e.g., *van Keken*, 1997] and the deformation and stirring patterns in mantle plume and the entrainment process of ambient mantle might be significantly influenced. Other effects such as the viscosity increase at 670-km discontinuity and phase changes would also affect the plume morphology and the corresponding stirring processes. Incorporation of these effects in future studies would help to elucidate these processes.

[12] **Acknowledgments.** We thank Henri Samuel and Allen K. McNamara for their helpful comments and detailed suggestions for the improvement of the manuscript, and Eric Calais for his comments. This study is supported by National Science Foundation and National Science Council, ROC.

References

Christensen, U. R., and A. W. Hofmann (1994), Segregation of subducted oceanic crust in the convecting mantle, *J. Geophys. Res.*, *99*, 19,867–19,884.

Davaille, A. (1999), Simultaneous generation of hotspots and superswells by convection in a heterogeneous planetary mantle, *Nature*, *402*, 756–760.

Davies, G. F. (1999), *Dynamic Earth: Plates, Plumes and Mantle Convection*, Cambridge Univ. Press, New York.

Davies, G. F. (2002), Stirring geochemistry in mantle convection models with stiff plates and slabs, *Geochim. Cosmochim. Acta*, *66*, 3125–3142.

Farnetani, C. G., and H. Samuel (2003), Lagrangian structures and stirring in the Earth's mantle, *Earth Planet. Sci. Lett.*, *206*, 335–348.

Farnetani, C. G., and H. Samuel (2005), Beyond the thermal plume paradigm, *Geophys. Res. Lett.*, *32*, L07811, doi:10.1029/2004GL022131.

Farnetani, C. G., B. Legras, and P. J. Tackley (2002), Mixing and deformations in mantle plumes, *Earth Planet. Sci. Lett.*, *196*, 1–15.

Ferrachat, S., and Y. Ricard (1998), Regular vs. chaotic mantle mixing, *Earth Planet. Sci. Lett.*, *155*, 75–86.

Hart, S. R., E. H. Hauri, L. A. Oschmann, and J. A. Whitehead (1992), Mantle plumes and entrainment: The isotopic evidence, *Science*, *256*, 517–520.

Hauri, E. H., J. A. Whitehead, and S. R. Hart (1994), Fluid dynamic and geochemical aspects of entrainment in mantle plumes, *J. Geophys. Res.*, *99*, 24,275–24,300.

Kellogg, L. H., and D. L. Turcotte (1990), Mixing and the distribution of heterogeneities in a chaotically mixing mantle, *J. Geophys. Res.*, *95*, 421–432.

Lin, S. C., and P. E. van Keken (2006a), Dynamics of thermochemical plumes: 1. Plume formation and entrainment of a dense layer, *Geochem. Geophys. Geosyst.*, *7*, Q02006, doi:10.1029/2005GC001071.

Lin, S. C., and P. E. van Keken (2006b), Dynamics of thermochemical plumes: 2. Complexity of plume structures and its implications for mapping mantle plumes, *Geochem. Geophys. Geosyst.*, *7*, Q03003, doi:10.1029/2005GC001072.

McNamara, A. K., and S. Zhong (2005), Thermochemical structures beneath Africa and the Pacific Ocean, *Nature*, *437*, 1136–1139.

Metcalfe, G., C. R. Bina, and J. M. Ottino (1995), Kinematic considerations for mantle mixing, *Geophys. Res. Lett.*, *22*, 743–746.

Ottino, J. M. (1989), *The Kinematics of Mixing: Stretching, Chaos, and Transport*, Cambridge University Press, New York.

Ren, Z.-Y., S. Ingle, E. Takahashi, N. Hirano, and T. Hirata (2005), The chemical structure of the Hawaiian mantle plume, *Nature*, *436*, 837–840.

Schmalzl, J., G. A. Houseman, and U. Hansen (1996), Mixing in vigorous, time-dependent, three-dimensional convection and application to Earth's mantle, *J. Geophys. Res.*, *101*, 21,847–21,858.

Tackley, P. J., and S. D. King (2003), Testing the tracer ratio method for modeling active compositional fields in mantle convective simulations, *Geochem. Geophys. Geosyst.*, *4*(4), 8302, doi:10.1029/2001GC000214.

Ten, A., D. A. Yuen, Y. Y. Podladchikov, T. B. Larsen, E. Pachepsky, and A. V. Malevsky (1997), Fractal features in mixing of non-Newtonian and Newtonian mantle convection, *Earth Planet. Sci. Lett.*, *146*, 401–414.

van der Hilst, R. D., and H. Kárason (1999), Compositional heterogeneity in the bottom 1000 kilometers of Earth's mantle: Toward a hybrid convection model, *Science*, *283*, 1885–1888.

van Keken, P. E. (1997), Evolution of starting mantle plumes: a comparison between numerical and laboratory models, *Earth Planet. Sci. Lett.*, *148*, 1–11.

van Keken, P. E., E. H. Hauri, and C. J. Ballentine (2002), Mantle mixing: The generation, preservation, and destruction of chemical heterogeneity, *Annu. Rev. Earth Planet. Sci.*, *30*, 493–525.

van Keken, P. E., C. Ballentine, and E. Hauri (2003), Convective mixing in the Earth's mantle, in *Treatise of Geochemistry,* vol. 2, *Geochemistry of the Mantle and Core*, edited by R. Carlson, pp. 471–491, Elsevier, New York.

White, W. M., A. R. McBirney, and R. A. Duncan (1993), Petrology and geochemistry of the Galapagos Islands: Portrait of a pathological mantle plume, *J. Geophys. Res.*, *98*, 19,533–19,563.

S.-C. Lin, Department of Geosciences, National Taiwan University, Taipei, Taiwan. (skylin0@ntu.edu.tw)

P. E. van Keken, Department of Geological Sciences, University of Michigan, Ann Arbor, MI 48109, USA. (keken@umich.edu)